

Towards imaging electron density inside metal–organic framework structures†

Yohei Takashima, De-Liang Long and Leroy Cronin*

Cite this: *Chem. Commun.*, 2014, 50, 2271Received 11th November 2013,
Accepted 16th December 2013

DOI: 10.1039/c3cc48586b

www.rsc.org/chemcomm

Herein, we present electron density maps of three MOFs with different guests or post-synthetic modifications produced using single crystal X-ray data from laboratory diffractometers. Analysis of the electron density maps reveals possible differences inside the pores indicating that this approach may be used to explore frameworks using inexpensively gained X-ray data.

Metal–Organic Frameworks (MOFs), or porous coordination polymers (PCPs), are crystalline porous materials constructed from the coordination bonds between metal ions and organic linkers, which have attracted considerable attention for their potential applications in gas storage, gas separation and catalysis.¹ One of the biggest advantages of MOFs compared to other conventional porous materials is their synthetic designability, and it is possible to modulate their pore size, shape and functionality with the judicious choice of metal nodes, organic linkers and synthetic strategies. Furthermore, post-synthetic modification (PSM) is also becoming an important method to functionalize the pores.²

In contrast to the development of their synthetic methodologies, the direct observation of host–guest interactions inside the pores is limited in spite of the crucial importance for understanding and improving their porous properties. When the pore size is small enough for guest molecules, it is possible to resolve some details of the interactions using conventional Fourier-difference map crystallographic approaches.³ However, it becomes intrinsically more difficult to explore the inner-space of larger or disordered structures, especially if conformationally mobile groups, weak binding sites, or statistically distributed reactive sites are included. This can be greatly exacerbated for embedded alkyl groups, which are almost impossible to be located in the structure refinement due to severe disorder.^{2d,4}

Herein, we explore the use of a direct-space electron density synthesis method to probe the guests and the structure of MOFs,

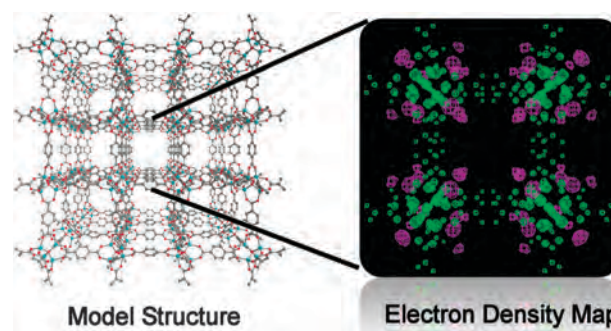


Fig. 1 Outline of the concept with a model (left) to electron density map (right) for $[\text{Zn}_4\text{O}(\text{bdc})_3]_n$. Hydrogen atoms and guests in the pores are omitted for clarity.

for example to investigate the incorporation of the disordered guest molecules inside the pores. Electron density maps can be used to show all the electron density data, rather than the difference maps traditionally used in small molecule crystallography. Indeed, the direct fitting of electron density is often used in protein crystallography to build the overall structural model,⁵ yet electron density maps of ‘small molecule’ structures like MOFs have not been examined and discussed in detail.⁶ In this work, the electron density maps were generated and analyzed using the VESTA software,⁷ see Fig. 1, which allowed us to, in preliminary studies, elucidate and compare the states inside the pores as a function of solvation, temperature, or post synthetic modification.

To develop this approach three ‘model’ MOFs were chosen: $[\text{Zn}_4\text{O}(\text{bdc})_3]_n$ (**1**, bdc = 1,4-benzene dicarboxylate), $[\text{Zn}_4\text{O}(\text{NH}_2\text{bdc})_3]_n$ (**2**, NH_2bdc = 2-amino-1,4-benzene dicarboxylate) and $[\text{Zn}_2(\text{bdc})_2\text{-dabco}]_n$ (**3**, dabco = diazabicyclo[2,2,2]octane) were prepared according to the reported methods.⁸ Compound **1** is the well-known MOF-5 compound and has a crystal structure where $[\text{Zn}_4\text{O}]^{6+}$ metal clusters are connected to octahedral arrays of bdc groups to form a cubic framework. Compound **2** is isostructural to **1** in which the 2-amino group is disordered over eight sites and the amino groups are available for PSM and the post-modified samples with alkyl or benzoic anhydrides were

WestCHEM, School of Chemistry, University of Glasgow, Glasgow, G12 8QQ, Scotland, UK. E-mail: Lee.Cronin@glasgow.ac.uk; Web: <http://www.croninlab.com>

† Electronic supplementary information (ESI) available: Experimental section, TGA, ¹H NMR, 2D electron density maps, intensity statistics dataset for X-ray measurements. See DOI: 10.1039/c3cc48586b

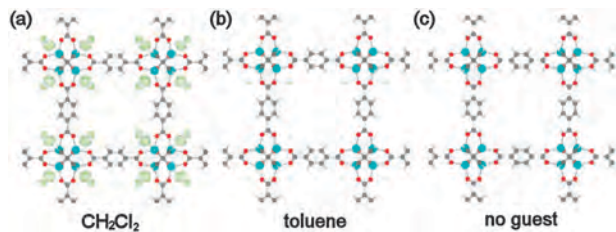


Fig. 2 Perspective view of 3D electron density maps ($F_o - F_c$) of **1** with (a) CH_2Cl_2 , (b) toluene as guests and (c) without guests at 150 K. $F_o - F_c$ maps are contoured at $1 \text{ e} \text{ \AA}^{-3}$ with green color. Gray, white, red and light blue are C, H, O and Zn, respectively.

also prepared to compare their electron density maps with each other. Compound **3** is a tetragonal framework in which 2D square-grid sheets are constructed by Zn paddle-wheel units and bdc are connected by dabco pillar ligands. Fig. 2 shows the electron density maps of **1** with different guests. The guests were successfully incorporated into the pores by a guest-exchange protocol, wherein the as-synthesized samples were soaked in a liquid of each of the guests. Their structures were refined only using framework atoms, indicating that the $F_o - F_c$ maps show the unassigned electron densities associated with solvent guests inside the pores.

In the cases where CH_2Cl_2 were included as guest molecules, a large amount of electron density was only observed close to zinc clusters despite the full accommodation of guests inside (according to TGA, see ESI[†]), indicating that some CH_2Cl_2 guests were localized on the corners and others were highly disordered in the pores (Fig. 2a). In contrast, almost no ordered electron density was found when the guest was toluene, and the map appeared to be similar to the empty MOF without guests, see Fig. 2b and c. This is because the difference can be explained by the properties of guests; CH_2Cl_2 guests are sterically small (33.9 \AA^3) and also have two acidic protons which facilitates interactions with the Lewis basic oxygen sites of Zn_4O clusters. In addition, the relatively high electron densities associated with the chlorine atoms in the CH_2Cl_2 make it easier to visualize, despite the presence of some disorder. On the other hand, the toluene guests are sterically large (101.32 \AA^3), and have no acidic protons, thereby having weaker interactions with the Zn_4O clusters. Fig. 3 shows the electron density maps of **2** with PSMs. PSMs are nowadays recognized as a very powerful method to modify the pore surface functionalities of MOFs after assembly. However, in most of the cases, the installed chemical moieties could not be located by using conventional single crystal diffraction experiments because of severe disorder, making it difficult to probe with the porous properties directly.^{2d,4}

Five post-modified samples of **2**, **2-AM1**, **2-AM4**, **2-AM6**, **2-AM13** and **2-AMbz**, were prepared according to the methods of Cohen *et al.*^{2d} Alkyl moieties with different chain length or benzene moiety were incorporated by amide bond formation with the corresponding anhydrides. The modifications were executed with CHCl_3 as solvent and CHCl_3 was then accommodated as the guest solvent in the resulting crystals. The conversions of the post-synthetic modifications were estimated by digestion of the single crystals of the compounds, followed by ^1H NMR measurements with the resulting solutions, see Table 1.

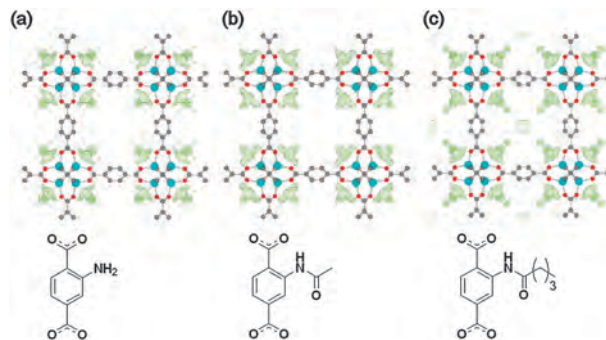


Fig. 3 Perspective view of 3D electron density maps ($F_o - F_c$) of **2** at 150 K: (a) no modification (**2**), modifications with (b) acetic anhydride (**2-AM1**) and (c) valeric anhydride (**2-AM4**). See ESI[†] for heptanoic anhydride (**2-AM6**), myristic anhydride (**2-AM13**) and benzoic anhydride (**2-AMbz**). Chemical structures of the resulting ligand moieties are shown below their maps, respectively. $F_o - F_c$ maps are contoured at $0.8 \text{ e} \text{ \AA}^{-3}$ with green color. Color codes for atoms on frameworks follow those of Fig. 2.

Table 1 Percent conversion of **2** with different anhydrides as determined by ^1H NMR

2	AM1	AM4	AM6	AM13	AMbz
Conversion	96%	79%	72%	31%	30%

In general, the nitrogen atoms on the ligands and installed chemical moieties by PSMs were not assigned crystallographically because of disorder, indicating that the $F_o - F_c$ maps include both contributions from installed chemical moieties and CHCl_3 guests, see Fig. 3. However, the $F_o - F_c$ maps did not show any indication of the installed chemical moieties, which indicates that they are highly disordered even at 150 K. By contrast, the electron density maps showed densities observed near the Zn_4O clusters, similar to the case of **1** with CH_2Cl_2 guests. The sterically small CHCl_3 (69.94 \AA^3) moiety with an acidic proton means that it should be localized near the Zn_4O cluster units.

It is noteworthy that the observed electron densities show a range of different sizes and shapes depending on the installed moieties by PSMs, indicating that installed moieties produce strong effects for pore functionalities. It is especially interesting that the electron densities are spread over a wider area near the cluster units for **2-AM13** and **2-AMbz** despite the lower conversions of the PSM process, see ESI[†]. In addition, in the case of **2-AM4** and **2-AM6**, electron density was also observed in the middle of the pores and higher conversions for PSMs with relatively long alkyl chains appear to be important to reduce disorder and indicate significant ordering within the pores, see ESI[†].

Fig. 4 shows the direct $F_o - F_c$ data from the line connecting (0, 0, 0) and (0.25, 0.25, 0.25), making it possible to compare the compounds in a more quantitative fashion. As expected from the 3D electron density maps shown in Fig. 3, electron density was observed near the middle of the pores (distance: 0 \AA) for **2-AM4** and **2-AM6**. On the other hand, the electron densities for **2** and **2-AM1** were quite low, indicating that the guests are highly disordered because of less steric hindrance inside. Interestingly, **2-AM13** also showed low electron densities despite the presence of long alkyl

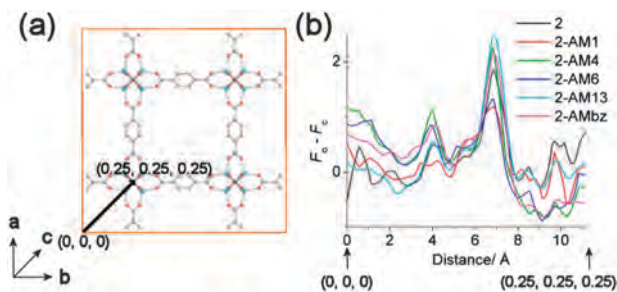


Fig. 4 (a) Line profile between (0, 0, 0) and (0.25, 0.25, 0.25). Color codes for atoms on frameworks follow those of Fig. 2. Orange line shows unit cell. (b) Plots of $F_o - F_c$ against the line shown in (a).

chains inside the pore, and it would be consistent if the moieties were localized near the Zn_4O clusters. In fact, the highest electron densities were observed near the clusters (distance: 6.9 Å) and higher electron densities were also observed near the clusters for **2-AM4** and **2-AMbz**, implying that guests would be more stabilized by their PSMs. The rigid benzene moieties in **2-AMbz** allow the guests to be stabilized efficiently. Interestingly, the electron densities for **2** were higher than those for **2-AM1** and **2-AM6**, and this is most likely due to the acid–base interactions between amino groups and the included guest molecules.

To understand the effect of temperature on the electron density maps, single X-ray diffraction measurements with **2-AM4** were carried out at different temperatures and their electron density maps were visualized, respectively (Fig. 5a–d). As expected, the electron densities around Zn_4O clusters became more featureless and smaller as the temperature increased. On the other hand, the electron densities on the center showed small changes in their shapes. Also, the line profile of $F_o - F_c$ shown in Fig. 5e indicates that the electron densities near clusters showed a clear decrease at 200 K and 250 K with a small increase around (distance: 4.5 to 6 Å), indicating that the $CHCl_3$ guests became more disordered by their thermal motion. Similar decreases were also observed near the centers, especially the sudden decrease at 250 K clearly indicates the higher disorder inside.

Finally, we produced electron density maps with **3** since, unlike the MOFs shown earlier, compound **3** has smaller pores, making it possible to stabilize the guests by strong host–guest interactions. Fig. 6 shows the electron density maps of **3** in which the guests were not assigned intentionally in the crystal structures, indicating that $F_o - F_c$ maps include the electron density contributions from the guests. As expected, the 3D electron density map clearly shows the DMF guests themselves, indicating that the DMF guests were localized in the pores (Fig. 6a). The advantage of visualizing electron density maps is that we can see not only their shapes but also the correlated intensities of electron density; even if their shapes of the electron densities look similar, differences in population can be mapped. This is demonstrated by 2D electron density maps of compound **3** at different temperatures which were produced in which only the electron densities on one plane perpendicular to the c axis were visualized, making it possible to analyze the electron densities inside easily.

As shown in Fig. 6b–d, the 2D electron density maps clearly showed that DMF guests were localized close to bdc ligands at all temperatures, however, their shapes and intensities were

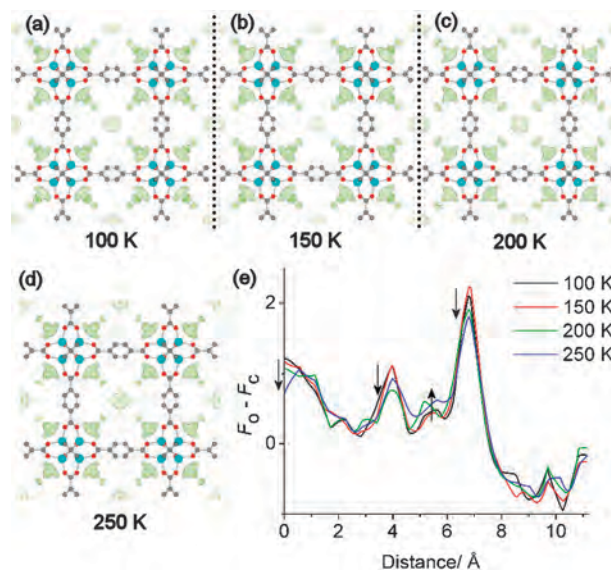


Fig. 5 Perspective view of 3D electron density maps ($F_o - F_c$) of **2-AM4** at different temperatures: (a) 100 K, (b) 150 K, (c) 200 K and (d) 250 K. $F_o - F_c$ maps are contoured at $0.8 \text{ e} \text{ \AA}^{-3}$ with green color. Color codes for atoms on frameworks follow those of Fig. 2. (e) Plots of $F_o - F_c$ against the line between (0, 0, 0) and (0.25, 0.25, 0.25).

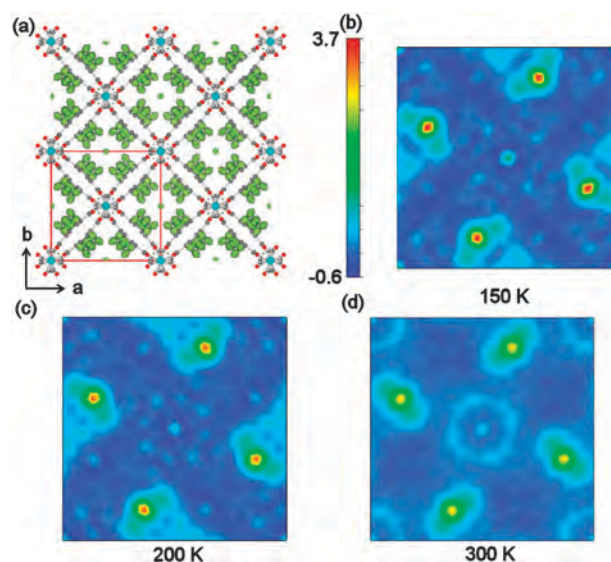


Fig. 6 Electron density maps ($F_o - F_c$) of **3** with DMF guests: (a) 3D electron density maps; $F_o - F_c$ maps are contoured at $1 \text{ e} \text{ \AA}^{-3}$ with green color. Red line shows unit cell. Color codes for atoms on frameworks follow those of Fig. 2. 2D electron density maps on the (003) plane at (b) 150 K, (c) 200 K and (d) 300 K, showing the stable location of electron density peaks with variation of temperatures.

different depending on the measurement temperatures; their characteristic shape with higher intensities became more featureless with lower intensities as the temperatures increased, indicating that DMF guests are more disordered because of their higher thermal motion as expected.

In conclusion, we have investigated the ‘inner space’ electron density of several ‘model’ MOFs with different guests or PSMs

and their electron density maps were very easily obtained using routine X-ray data from standard laboratory diffractometers. As such we believe this approach is interesting for the field as it is currently underutilizing the available X-ray data. This is because this approach for instance showed that it was possible to explore the characteristics of the included guests/PSM and the electron density analysis gives much more information than is not normally available from standard crystallographic methods including the observations that: (1) the guests with acidic protons were localized near the zinc cluster motifs; (2) the PSMs with bigger or more rigid moieties could make the guests more stabilized; (3) 2D electron density maps showed more clearly how guests become disordered at higher temperatures. This research therefore opens up the way for researchers to use X-ray data collected from conventional laboratory equipment to help evaluate the nature of the as-synthesized and crystallized MOFs, as well as to aid modeling approaches/simulations used to explore the 'inner-space' of many MOFs in an effort to understand, design and predict their physical properties (as well as to discuss the limitations of such an approach).⁹ We are now attempting to develop model systems to directly compare both routine laboratory and high intensity/high resolution data gained from synchrotron sources.

We thank the ESPRC, WestCHEM, and University of Glasgow. L.C. thanks the Royal Society and the Wolfson Foundation for a Merit Award.

Notes and references

- (a) O. M. Yaghi, M. O'Keeffe, N. W. Ockwig, H. K. Chae, M. Eddaoudi and J. Kim, *Nature*, 2003, **423**, 705; (b) S. Kitagawa, R. Kitaura and S. Noro, *Angew. Chem., Int. Ed.*, 2004, **43**, 2334; (c) G. Férey, C. Mellot-Draznieks, C. Serre and F. Millange, *Acc. Chem. Res.*, 2005, **38**, 217; (d) D. Bradshaw, J. B. Claridge, E. J. Cussen, T. J. Prior and M. J. Rosseinsky, *Acc. Chem. Res.*, 2005, **38**, 273; (e) O. K. Farha and J. T. Hupp, *Acc. Chem. Res.*, 2010, **43**, 1166; (f) D. Zacher, O. Shekhah, C. Woll and R. A. Fischer, *Chem. Soc. Rev.*, 2009, **38**, 1418.
- (a) Z. Wang and S. M. Cohen, *Chem. Soc. Rev.*, 2009, **38**, 1315; (b) J. S. Seo, D. Whang, H. Lee, S. I. Jun, J. Oh, Y. J. Jeon and K. Kim, *Nature*, 2000, **404**, 982; (c) Z. Wang and S. M. Cohen, *J. Am. Chem. Soc.*, 2007, **129**, 12368; (d) K. K. Tanabe, Z. Wang and S. M. Cohen, *J. Am. Chem. Soc.*, 2008, **130**, 8508; (e) Y. Goto, H. Sato, S. Shinkai and K. Sada, *J. Am. Chem. Soc.*, 2008, **130**, 14354; (f) T. Gadzikwa, G. Lu, C. L. Stern, S. R. Wilson, J. T. Hupp and S. T. Nguyen, *Chem. Commun.*, 2008, 5493; (g) T. Haneda, M. Kawano, T. Kawamichi and M. Fujita, *J. Am. Chem. Soc.*, 2008, **130**, 1578; (h) M. J. Ingleson, J. P. Barrio, J.-B. Guilhaud, Y. Z. Khimiyak and M. J. Rosseinsky, *Chem. Commun.*, 2008, 2680; (i) Y.-F. Song and L. Cronin, *Angew. Chem., Int. Ed.*, 2008, **47**, 4635.
- (a) R. Kitaura, S. Kitagawa, Y. Kubota, T. C. Kobayashi, K. Kindo, Y. Mita, A. Matsuo, M. Kobayashi, H.-C. Chang, T. C. Ozawa, M. Suzuki, M. Sakata and M. Takata, *Science*, 2002, **298**, 2358; (b) R. Matsuda, R. Kitaura, S. Kitagawa, Y. Kubota, R. V. Belosludov, T. C. Kobayashi, H. Sakamoto, T. Chiba, M. Takata, Y. Kawazoe and Y. Mita, *Nature*, 2005, **436**, 238; (c) J.-P. Zhang and X.-M. Chen, *J. Am. Chem. Soc.*, 2009, **131**, 5516; (d) R. Vaidhyanathan, S. S. Iremonger, G. K. H. Shimizu, P. G. Boyd, S. Alavi and T. K. Woo, *Science*, 2010, **330**, 650; (e) E. D. Bloch, W. L. Queen, R. Krishna, J. M. Zadrozny, C. M. Brown and J. R. Long, *Science*, 2012, **335**, 1606.
- (a) Z. Wang and S. M. Cohen, *J. Am. Chem. Soc.*, 2009, **131**, 16675; (b) S. Henke, R. Schmid, J.-D. Grunwaldt and R. A. Fischer, *Chem.-Eur. J.*, 2010, **16**, 14296; (c) S. Henke, A. Schneemann, A. Wutscher and R. A. Fischer, *J. Am. Chem. Soc.*, 2012, **134**, 9464.
- L. Kohlstaedt, J. Wang, J. Friedman, P. Rice and T. Steitz, *Science*, 1992, **256**, 1783.
- (a) M. Yoshizawa, T. Kusukawa, M. Kawano, T. Ohhara, I. Tanaka, K. Kurihara, N. Niimura and M. Fujita, *J. Am. Chem. Soc.*, 2005, **127**, 2798; (b) J. L. C. Rowsell, E. C. Spencer, J. Eckert, J. A. K. Howard and O. M. Yaghi, *Science*, 2005, **309**, 1350; (c) L.-H. Xie, J.-B. Lin, X.-M. Liu, Y. Wang, W.-X. Zhang, J.-P. Zhang and X.-M. Chen, *Inorg. Chem.*, 2010, **49**, 1158.
- K. Momma and F. Izumi, *J. Appl. Crystallogr.*, 2011, **44**, 1272.
- (a) D. Saha, Z. Wei and S. Deng, *Sep. Purif. Technol.*, 2009, **64**, 280; (b) J. L. C. Rowsell and O. M. Yaghi, *J. Am. Chem. Soc.*, 2006, **128**, 1304; (c) D. N. Dybtsev, H. Chun and K. Kim, *Angew. Chem., Int. Ed.*, 2004, **43**, 5033.
- (a) T. Duren, Y.-S. Bae and R. Q. Snurr, *Chem. Soc. Rev.*, 2009, **38**, 1237; (b) C. E. Wilmer, M. Leaf, C. Y. Lee, O. K. Farha, B. G. Hauser, J. T. Hupp and R. Q. Snurr, *Nat. Chem.*, 2012, **4**, 83; (c) R. B. Getman, Y.-S. Bae, C. E. Wilmer and R. Q. Snurr, *Chem. Rev.*, 2011, **112**, 703.